to β-2-microglobulin mRNA. *$p<0.05$, **$p<0.01$(n=3).


Figure 4

Soft x-ray features of the transplanted complexes. A: 1 week after transplantation of control complex (GS-β/COFs). B: 1 week after transplantation of GS-β/BMP-2/COFs. C: 2 weeks after transplantation of control complex (GS-β/COFs). D: 2 weeks after transplantation of GS-β/BMP-2/COFs. E: 2 weeks after transplantation of GS-β/BMP-2.


Figure 5

Histology of transplanted complexes. A-F and H are undecalcified sections and G is decalcified paraffin section prepared as described in Materials and Methods. A: Histology of transplanted control complex (GS-β/COFs) after 1 week of the transplantation. Note that mineralized GS-β (brown to black) and non-mineralized GS-β (pink) are observed, but no ALP-positive cells are observed. B: Histology of transplanted GS-β/BMP-2/COFs complex after 1 week of the transplantation. Note that ALP-positive cells (blue) are observed around mineralized GS-β/bone (brown to black). C, D: Histology of transplanted GS-β/BMP-2 complex after 2 weeks of the transplantation. ALP-positive cells (blue) are observed around mineralized bone (brown to black). D is a higher magnification of C. E, F: Histology of transplanted GS-β/BMP-2/COFs complex after 2 weeks of the transplantation. Note that Numerous ALP-positive cells (blue) are observed around mineralized bone (brown to black). G: Histology of decalcified section of the transplanted GS-β/BMP-2/COFs complex after 2 weeks of the transplantation. Numerous osteocytes are embedded in bone matrices. Hematoxylin and eosin stain. H, I: Cartilage appeared in the transplants of GS-β/BMP-2

complex (H) and GS-β/BMP-2/COFs complex (I) after 2 weeks of the transplantation. Alcian blue stain. Bars: 100μm in A, B, C and E, 50 μm in E, 25 μm in D, F, G, H and I.


Figure 6

Localization of ALP-positive cells and GFP-positive cells in the ectopically formed bones at 2 weeks after transplantation of GS-β/BMP-2/COFs complex. GFP-positive cells were monitored before staining both ALP and von Kossa. Blue cells in A and C are ALP-positive cells, and mineralized bone is shown in brown. Pictures of B and D were taken by fluorescence microscope. Green cells in B and D are GFP-positive cells. Red arrows indicate the cells showing both positive for ALP and GFP, and yellow arrows indicate the cells showing GFP-positive but ALP-negative. Pink asterisks indicate the rests of GS-β. Bars indicate 20μm.
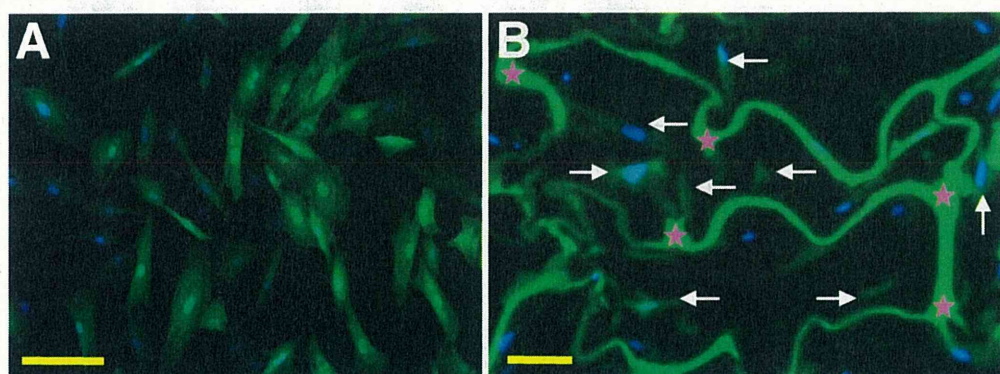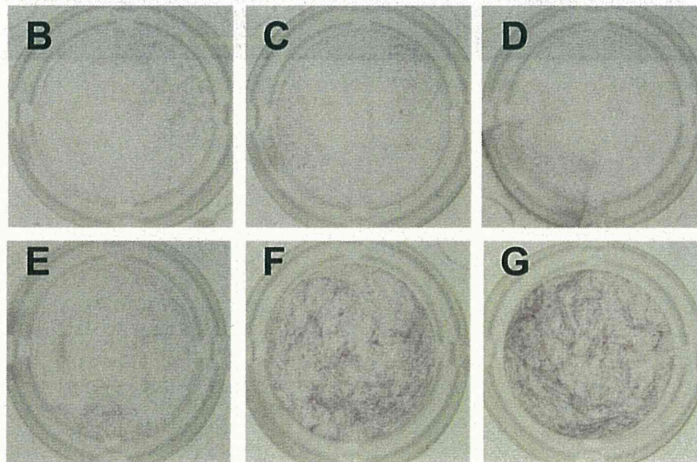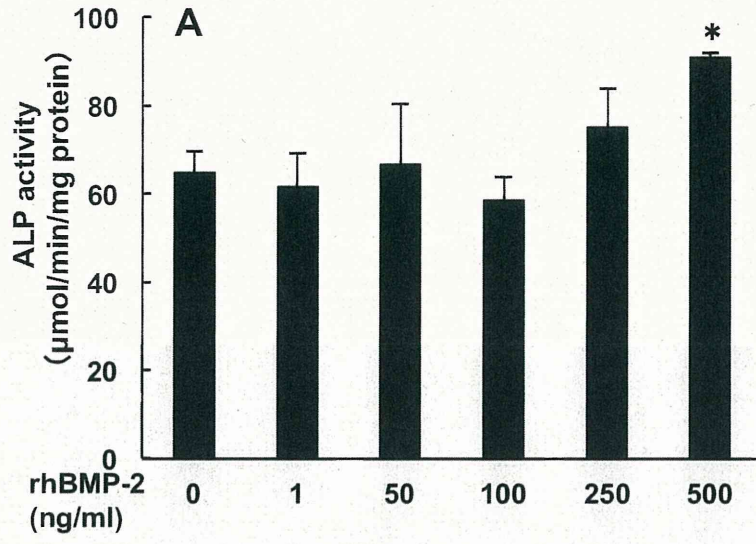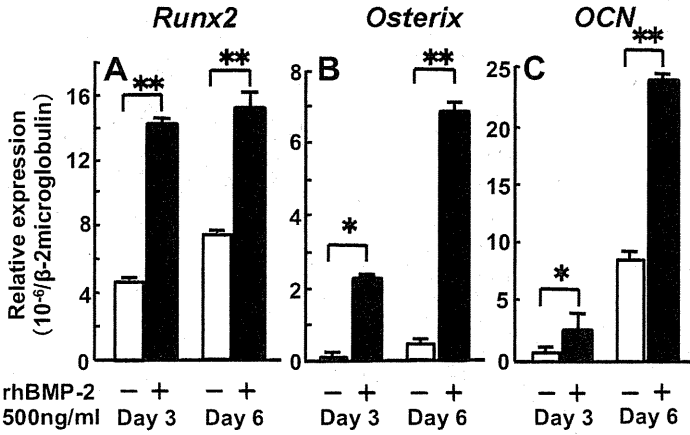
# Figure 1

**Figure 2**

# Figure 3

# Figure 4
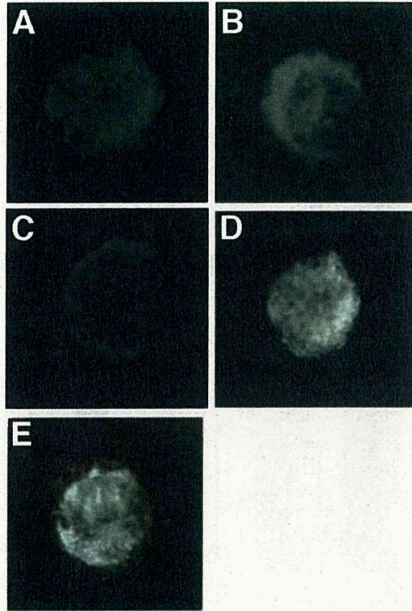
**Figure 5**
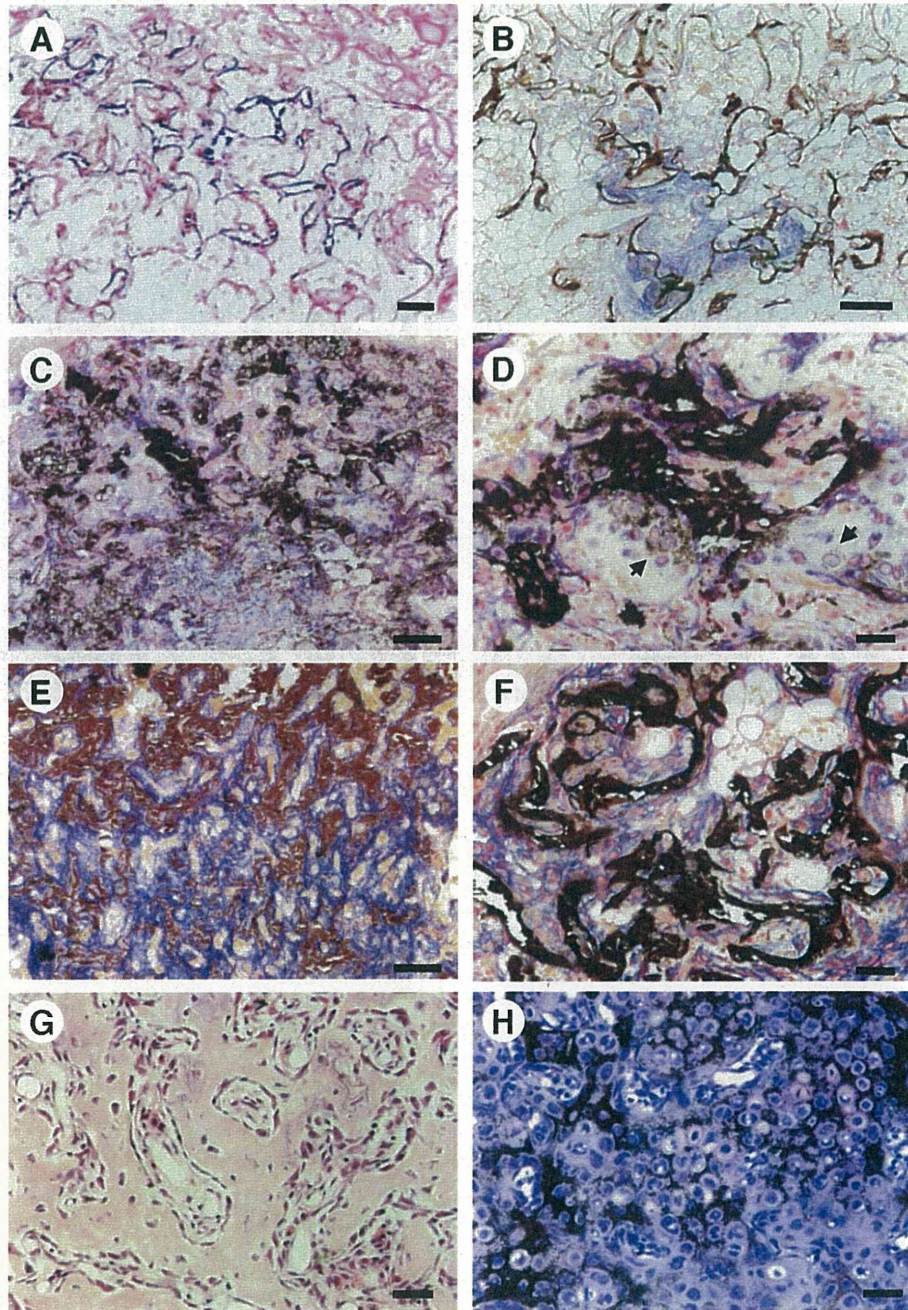
# Figure 6
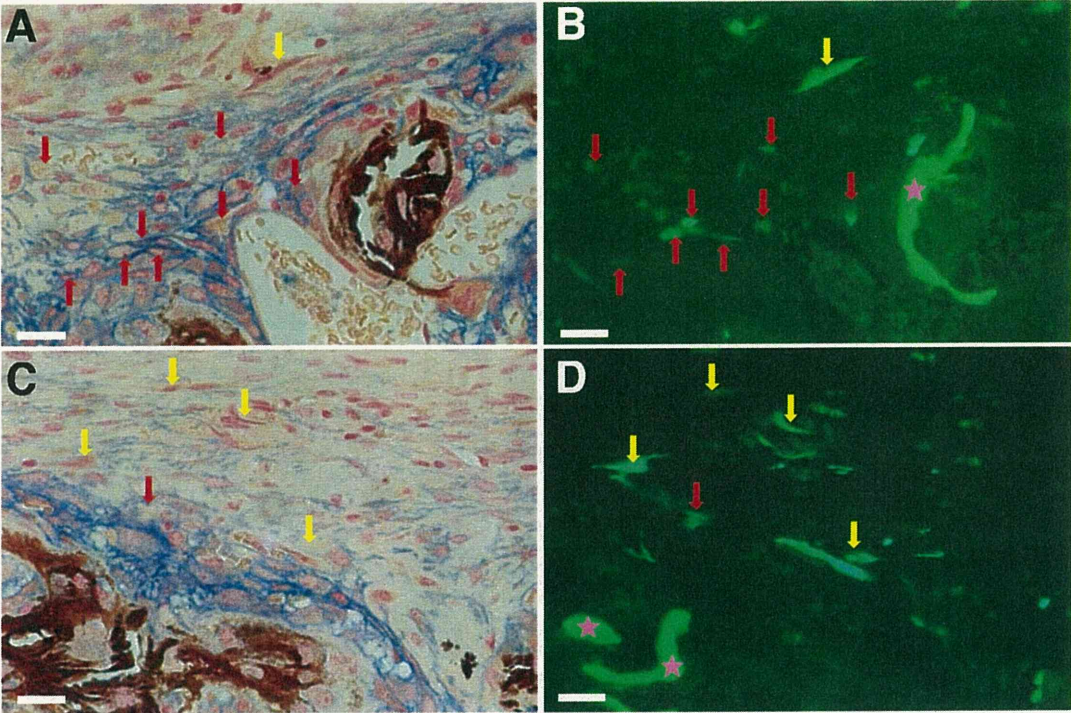
# Cdc42 is required for chondrogenesis and interdigital programmed cell death during limb development ☆

Ryo Aizawa [a,b], Atsushi Yamada [a,*], Dai Suzuki [a], Tadahiro Iimura [c],
Hidetoshi Kassai [d,e], Takeshi Harada [d,e], Masayuki Tsukasaki [a], Gou Yamamoto [f],
Tetsuhiko Tachikawa [f], Kazuki Nakao [e,g], Matsuo Yamamoto [b], Akira Yamaguchi [c],
Atsu Aiba [d,e], Ryutaro Kamijo [a]

[a] Department of Biochemistry, School of Dentistry, Showa University, Shinagawa-ku, Tokyo 142-8555, Japan
[b] Department of Periodontology, School of Dentistry, Showa University, Ohta-ku, Tokyo 142-8555, Japan
[c] Global Center of Excellence (GCOE) Program, International Research Center for Molecular Science in Tooth and Bone Diseases, Section of Oral Pathology, Tokyo Medical and Dental University, Bunkyo-ku, Tokyo 113-8549, Japan
[d] Division of Molecular Genetics, Department of Physiology and Cell Biology, Kobe University Graduate School of Medicine, Kobe, Hyogo 650-0017, Japan
[e] Laboratory of Animal Resources, Center for Disease Biology and Integrative Medicine, Faculty of Medicine, University of Tokyo, Bunkyo-ku, Tokyo 113-0033, Japan
[f] Department of Oral Pathology and Diagnosis, School of Dentistry, Showa University, Shinagawa-ku, Tokyo 142-8555, Japan
[g] Laboratory for Animal Resources and Genetic Engineering, RIKEN Center for Developmental Biology, Kobe, Hyogo 650-0047, Japan

## ARTICLE INFO

## ABSTRACT

Cdc42, a member of the Rho subfamily of small GTPases, is known to be a regulator of multiple cellular functions, including cytoskeletal organization, cell migration, proliferation, and apoptosis. However, its tissue-specific roles, especially in mammalian limb development, remain unclear. To investigate the physiological function of Cdc42 during limb development, we generated limb bud mesenchyme-specific inactivated Cdc42 ($Cdc42^{fl/fl}$; Prx1-Cre) mice. $Cdc42^{fl/fl}$; Prx1-Cre mice demonstrated short limbs and body, abnormal calcification of the cranium, cleft palate, disruption of the xiphoid process, and syndactyly. Severe defects were also found in long bone growth plate cartilage, characterized by loss of columnar organization of chondrocytes, and thickening and massive accumulation of hypertrophic chondrocytes, resulting in delayed endochondral bone formation associated with reduced bone growth. In situ hybridization analysis revealed that expressions of Col10 and Mmp13 were reduced in non-resorbed hypertrophic cartilage, indicating that deletion of Cdc42 inhibited their terminal differentiation. Syndactyly in $Cdc42^{fl/fl}$; Prx1-Cre mice was caused by fusion of metacarpals and a failure of interdigital programmed cell death (ID-PCD). Whole mount in situ hybridization analysis of limb buds showed that the expression patterns of Sox9 were ectopic, while those of Bmp2, Msx1, and Msx2, known to promote apoptosis in the interdigital mesenchyme, were down-regulated. These results demonstrate that Cdc42 is essential for chondrogenesis and ID-PCD during limb development.

## 1. Introduction

The skeleton of vertebrate limbs develops from limb buds that are initially composed of undifferentiated mesenchymal cells covered by ectoderm. The skeletal pattern is predetermined during a relatively early phase of limb development by pre-cartilaginous condensation, in which mesenchymal cells are recruited to form aggregates (Capdevila and Izpisua Belmonte, 2001; Niswander, 2003; Tickle, 2002). The molecular mechanisms governing condensation are not fully understood, though several genes have been implicated in this process (DeLise et al., 2000; Hall and Miyake, 2000). Mesenchymal cells differentiate into connective tissues including tendons, ligaments, and chondrocytes, which form cartilage templates based on the limb skeleton (Francis-West et al., 2003; Oldfield and Evans, 2003). Outgrowth of the limb skeleton is regulated by the coordinated expansion and differentiation of chondrocytes in the growth plate through a process known as endochondral ossification. During endochondral ossification, chondrocytes proliferate, undergo hypertrophy and die; the last of which deposit bone on remnants of the cartilage matrix (Erlebacher et al., 1995; Karsenty, 2003; Kronenberg, 2003).

During limb development, programmed cell death (PCD) of interdigital mesenchyme is a predictable process for digit separation in vertebrate species with free digits, and is controlled by a variety of signals that result in distinct temporal and special areas in which cells die (Hernandez-Martinez and Covarrubias, 2011). Among the variety of signals involved in interdigital programmed cell death (ID-PCD), bone morphogenetic proteins (Bmps) play pivotal roles, and are required to separate digits and prevent soft tissue syndactyly (Robert, 2007). Bmps, including Bmp2, Bmp4, and Bmp7, are involved in early patterning (Bastida et al., 2009; Maatouk et al., 2009; Pizette et al., 2001), as well as bone and cartilage formation (Macias et al., 1997; Pizette et al., 2001; Zou et al., 1997), joint specification (Merino et al., 1999), and PCD signals for both the ectoderm of the apical ectodermal ridge (AER) and mesoderm (Robert, 2007). Homeobox genes, including the Msx genes Msx1 and Msx2, downstream targets of BMP signaling, are expressed in the major areas of PCD in developing limbs, which indicates that they have roles as positive regulators of PCD (Chen and Zhao, 1998; Ovchinnikov et al., 2006).

The Rho family of small GTPases are molecular switches that control a wide variety of signal transduction pathways in all eukaryotic cells (Bishop and Hall, 2000). RhoA, Rac1, and Cdc42 are the best characterized members of small Rho GTPases, of which Cdc42 plays pivotal roles in regulating actin cytoskeleton, cell polarity, microtubule dynamics, membrane transport pathways, and transcription factor activity (Burridge and Wennerberg, 2004; Etienne-Manneville and Hall, 2002). Recently, the in vivo functions of Cdc42 were demonstrated using tissue-specific Cdc42 knockout mice (Cdc42 conditional knockout mice), as Cdc42 global knockout mice show embryonic lethality and die before embryonic day (E) 7.5 (Chen et al., 2000; Heasman and Ridley, 2008; Melendez et al., 2011). Cdc42-null embryonic stem cells show defects in organization of the actin cytoskeleton, including a failure of filopodia formation (Chen et al., 2000).

Several studies have shown that Cdc42 plays important roles in chondrocyte biology, including chondrogenesis, chondrocyte proliferation, hypertrophy, and apoptosis (Wang and Beier, 2005; Woods et al., 2007b). Furthermore, a recent comprehensive examination of the role of Cdc42 in osteoclast regulation in mouse models found that Cdc42 regulates the receptor activator of nuclear factor kappa-B ligand (RANKL)-mediated bone resorption process (Ito et al., 2010). However, little is known about the function of Cdc42 in chondrogenesis in vivo and during limb development. To investigate the roles of Cdc42 at various stages of limb patterning and skeletogenesis, we used a well-characterized transgene in which Cre-recombinase is expressed under the control of the Prx1 limb enhancer (Logan et al., 2002). This transgene expresses Cre very early in limb development, resulting in complete recombination of floxed alleles in early limb bud stages. We previously demonstrated that inactivation of Rac1, a Rho GTPase member, in mouse limb bud mesenchyme by use of a conditional floxed allele of Rac1 and the Prx1-Cre transgene led to skeletal deformities in the autopod and soft tissue syndactyly, with the latter caused by a complete absence of ID-PCD. Those findings in Rac1 conditional knockout mice (Rac1$^{fl/fl}$; Prx1-Cre) indicate crucial roles for Rac1 in limb bud morphogenesis, especially ID-PCD (Suzuki et al., 2009).

In the present study, Cdc42 conditional knockout mice (Rac1$^{fl/fl}$; Prx1-Cre) showed short limbs, caused by a failure of endochondral ossification, and syndactyly, caused by fusion of metacarpals and failure to remove interdigital limb mesenchymal cells by PCD. Our findings suggest that Cdc42 is essential for chondrogenesis and limb bud ID-PCD.

## 2. Results

### 2.1. Generation of Cdc42 conditional mutants and inactivation of Cdc42 in limb mesenchyme

In the present study, we employed a Cre–loxP system for limb bud mesenchyme-specific inactivation of the Cdc42 gene using Prx1-Cre mice (Fig. 1A), since no Cdc42$^{-/-}$ offspring were born and no Cdc42$^{-/-}$ embryos were recovered early in embryogenesis (Chen et al., 2000). Mice with a conditional (floxed) mutation in both alleles of the Cdc42 gene (Cdc42 flox mice, Cdc42$^{fl/fl}$ mice) were crossed with mice expressing Cre recombinase under the control of a Prx1 limb enhancer to obtain Cdc42$^{fl/+}$; Prx1-Cre mice. Then, Cdc42$^{fl/+}$; Prx1-Cre mice males were crossed with Cdc42$^{fl/fl}$ females to obtain Cdc42$^{fl/fl}$; Prx1-Cre mice, while Cdc42$^{fl/fl}$ mice from this crossing were used as controls.

To verify recombination of the Cdc42 conditional allele by Cre leading to the Δexon2 allele of the Cdc42 gene, we used PCR and Western blot analyses of genomic DNA and protein isolated from limb buds at E12.5 (Fig. 1B), and E11.5 and E12.5 (Fig. 1C). To investigate the expression patterns and levels of Cdc42 in Cdc42$^{fl/fl}$ and Cdc42$^{fl/fl}$; Prx1-Cre mice, we performed whole-mount in situ hybridization analysis using limb buds obtained at E11.5, E12.5, and E13.5. A distinct expression of Cdc42 was observed in the interdigital region of the Cdc42$^{fl/fl}$ limb buds at E12.5 and E13.5. However, that
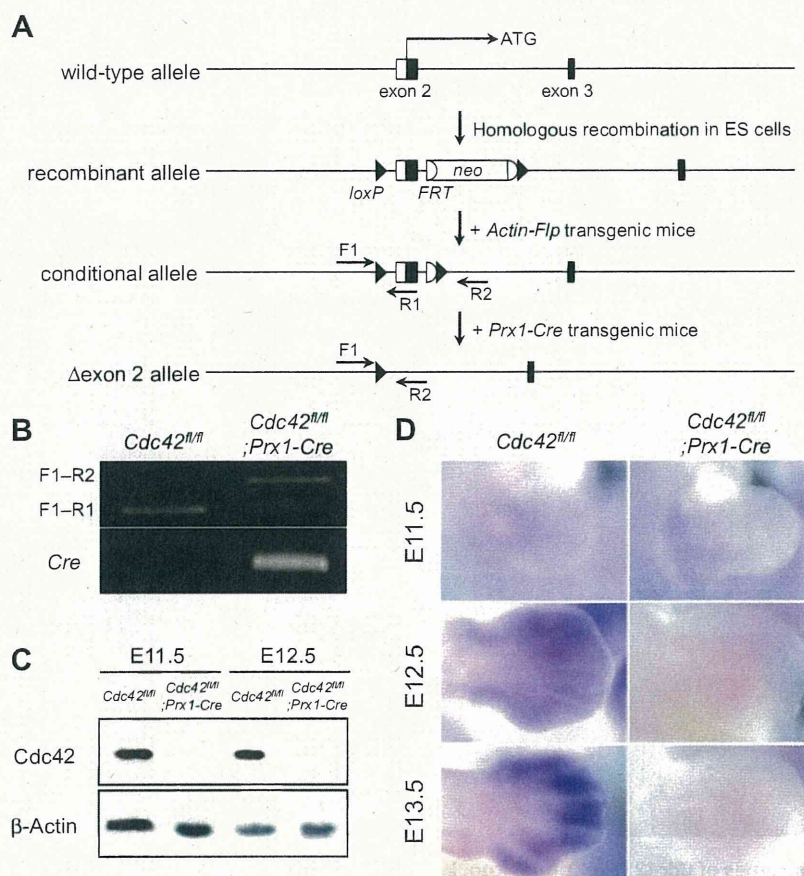
Fig. 1 – Generation of *Cdc42* conditional knockout mice. (A) Schematic drawing of targeting strategy for production of *Cdc42* conditional knockout mice. Different primers (F1, R1 and R2) were used for PCR assessment of *Cdc42* exon2 deletion (Δexon2). (B) Samples for PCR were obtained from *Cdc42$^{fl/fl}$* and *Cdc42$^{fl/fl}$*; *Prx1-Cre* limb buds obtained at E12.5. Conditional allele-specific (F1–R1; 162 bp) and Δexon2 allele-specific (F1–R2; 350 bp) bands were detected. A band for the *Prx-1-Cre* transgene (*Cre*) was detected only in *Cdc42$^{fl/fl}$*; *Prx1-Cre* embryos. (C) Western blot analysis for Cdc42 was performed using limb buds from *Cdc42$^{fl/fl}$* and *Cdc42$^{fl/fl}$*; *Prx1-Cre* embryos obtained at E11.5 and E12.5. Equal protein loading was documented by blotting for β-Actin at the same stages. (D) Whole-mount *in situ* hybridization analysis of *Cdc42* was performed at the indicated embryonic stages. All panels present dorsal views of forelimb buds from *Cdc42$^{fl/fl}$* and *Cdc42$^{fl/fl}$*; *Prx1-Cre* embryos, anterior to the top, and are shown at the same scale.

expression was scarcely detected in the *Cdc42$^{fl/fl}$*; *Prx1-Cre* limb buds (Fig. 1D).

## 2.2. *Cdc42* conditional mutants have severe skeletal defects

*Cdc42$^{fl/fl}$*; *Prx1-Cre* neonates appeared weaker and smaller, and no milk was found in their stomachs as compared to their *Cdc42$^{fl/fl}$* littermates (black arrows in Fig. 2A). Although most of the *Cdc42$^{fl/fl}$*; *Prx1-Cre* neonates were viable at birth, more than 90% (42 of 46) died within a few days. *Cdc42$^{fl/fl}$*; *Prx1-Cre* mice, which remained alive until the weaning stage, had shorter limbs and body as compared to their *Cdc42$^{fl/fl}$* littermates (Fig. 2B). To perform anatomical analysis, we subjected skeleton preparations of *Cdc42$^{fl/fl}$* and *Cdc42$^{fl/fl}$*; *Prx1-Cre* neonates to Alcian blue, which stains all cartilaginous elements, and Alizarin red, which stains mineralized bone matrix (Summary of phenotypes in Table S1). Those findings

demonstrated that *Cdc42$^{fl/fl}$*; *Prx1-Cre* mice had abnormal calcification of the craniums, including frontal, parietal, and interparietal bone (black arrow in Fig. 2C), as also seen in micro-computed tomography images (white arrow in Fig. 2C). More than 85% of the *Cdc42$^{fl/fl}$*; *Prx1-Cre* mice (40 of 46) demonstrated a cleft palate (black arrowhead in Fig. 2D) and there was no fusion of the secondary palate. Histological analyses of postnatal day 0 (P0) *Cdc42$^{fl/fl}$*; *Prx1-Cre* mice showed a failure of palatal shelf elongation for the process of palate closure, whereas completed palatal fusion was observed in *Cdc42$^{fl/fl}$* mice (black arrows in Fig. 2E). In addition, Cre recombinase activity was observed in the palates of *Prx1-Cre* transgenic mice at E13.5 (Fig. S1). We considered that a suckling disorder is caused by the cleft palate in *Cdc42$^{fl/fl}$*; *Prx1-Cre* mice, which may be a reason for their early neonatal mortality (black arrow in Fig. 2A). Furthermore, the sternal bar was frequently bifurcated, while the xiphoid process was malformed or lost in these mice (black arrowhead in Fig. 2F).
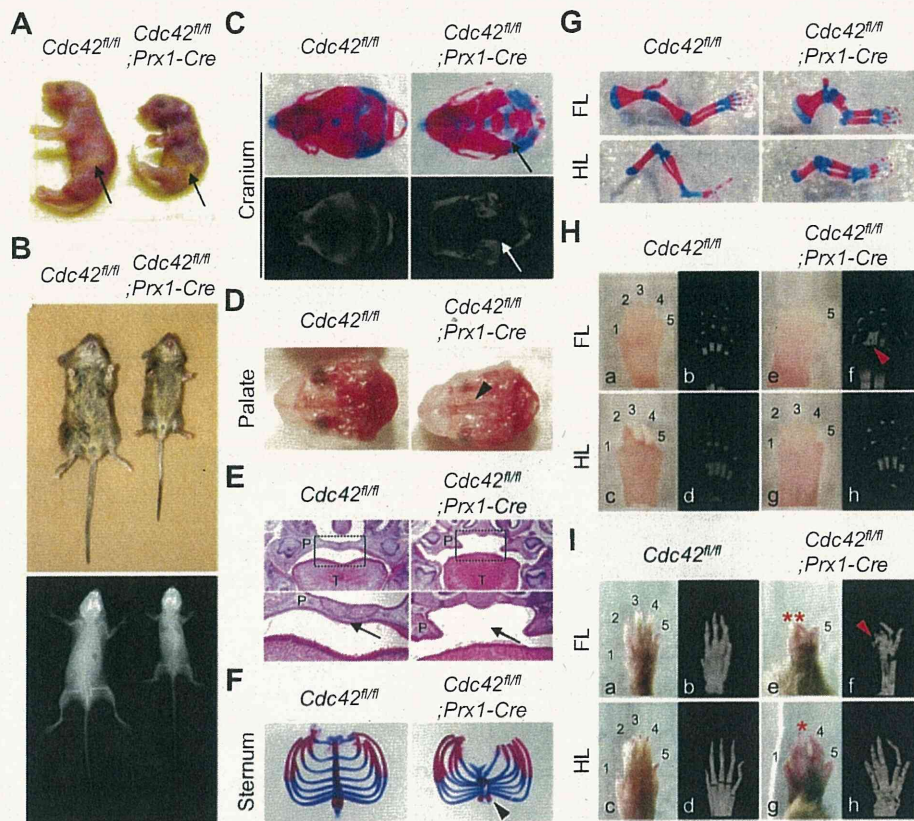
Fig. 2 – Skeletal phenotypes of Cdc42 conditional knockout mice. (A) Gross morphology at postnatal day 0 (P0). $Cdc42^{fl/fl}$; Prx1-Cre neonates demonstrated shortening of the limbs and body as compared to $Cdc42^{fl/fl}$ littermates. No milk was observed in the stomachs of $Cdc42^{fl/fl}$; Prx1-Cre mice (black arrows). (B) Gross morphology at P18. $Cdc42^{fl/fl}$; Prx1-Cre mice at the weaning stage demonstrated shortening of the limbs and body as compared to $Cdc42^{fl/fl}$ littermates (upper panels). Representative X-ray radiographs of a whole body (lower panels). (C) Alcian blue- and Alizarin red-stained skeletal preparations (upper panels), and micro-computed tomography images (lower panels) of dorsal views of skulls obtained at P0. Retarded fusion was seen in the fontanel of $Cdc42^{fl/fl}$; Prx1-Cre mice (black arrow in upper panel, white arrow in lower panel). (D) $Cdc42^{fl/fl}$; Prx1-Cre mice had a cleft palate at P0 (black arrowhead). (E) Hematoxylin- and Eosin-stained transverse histological sections from P0 mice. Palatal shelves were fully fused in $Cdc42^{fl/fl}$ mice, but not in $Cdc42^{fl/fl}$; Prx1-Cre mice (black arrows). Boxed areas are enlarged in the lower panels. P, palate; T, tongue. (F) Alcian blue- and Alizarin red-stained skeletal preparations of flat mounted dissected ribs from P0 mice. Disruption of the xiphoid process was seen in $Cdc42^{fl/fl}$; Prx1-Cre mice (black arrowhead). (G) Alcian blue- and Alizarin red-stained skeletal preparations of forelimbs (FL) and hindlimbs (HL) from P0 mice. (H) Gross observations and micro-computed tomography images of P0 mice FL and HL. Fusion of the 2nd and 3rd metacarpals was seen in the FL (red arrowhead in f), but not the HL of $Cdc42^{fl/fl}$; Prx1-Cre mice (h). (I) Gross observations and micro-computed tomography images of P18 mice FL and HL. Severe malformation and hypoplasia were seen in $Cdc42^{fl/fl}$; Prx1-Cre FL (double red asterisks in e). Soft tissue syndactyly was seen in $Cdc42^{fl/fl}$; Prx1-Cre HL (single red asterisks in g). Fusion of the phalange between the 2nd and 3rd digits was seen in the FL of $Cdc42^{fl/fl}$; Prx1-Cre mice (red arrowhead in f), but not the HL of $Cdc42^{fl/fl}$; Prx1-Cre mice (h).

All of the present $Cdc42^{fl/fl}$; Prx1-Cre mice had developmental defects in both the fore- and hindlimbs. $Cdc42^{fl/fl}$; Prx1-Cre neonates had shorter and thicker mineralized bones in the fore- and hindlimbs as compared to their $Cdc42^{fl/fl}$ littermates (Fig. 2G). The most striking feature of the limbs in $Cdc42^{fl/fl}$; Prx1-Cre mice was deformity, as the neonates had short, thick, and webbed limbs, and micro-computed tomography images of the forelimbs indicated fusion of the 2nd and 3rd metacarpales (red arrowhead in Fig. 2Hf). On the other hand, no fusion of the phalanges/metatarsals in $Cdc42^{fl/fl}$; Prx1-Cre hindlimbs was observed (Fig. 2Hh). Furthermore, $Cdc42^{fl/fl}$; Prx1-Cre forelimbs obtained at P18 showed syndactyly caused by fusion of the phalanges/metatarsals (Fig. 2Ie and f). On the other hand, $Cdc42^{fl/fl}$; Prx1-Cre hindlimbs showed soft tissue syndactyly, while no fusion of the phalanges/metatarsals in their hindlimbs was observed (Fig. 2Ig and h). Cdc42 deficient forelimb buds were more severely affected than the hindlimb buds, a result in line with the more robust Prx1-Cre activity occurring in the emerging forelimb than in the hindlimb bud (Logan et al., 2002).

### 2.3. Defects in growth plate development in Cdc42 conditional mutants

Development of the long bones was also affected in $Cdc42^{fl/fl}$; Prx1-Cre mice (Fig. 2G). To analyze the phenotypes of the long

bones in detail, we performed histological analyses of $Cdc42^{fl/fl}$; $Prx1$-$Cre$ neonates. Disorganized growth plates with wider hypertrophic cartilage and columnar disorganization of the proliferating and hypertrophic chondrocytes were seen in neonates, while non-resorbed hypertrophic cartilage remained in growth plates (Fig. 3A and B). In situ hybridization analyses of $Cdc42^{fl/fl}$; $Prx1$-$Cre$ tibiae obtained at E18.5 showed that the expression levels of Col10 and Mmp13 were reduced, while that of Col2 was not different as compared to $Cdc42^{fl/fl}$ control (Fig. 3C–E). These results indicate that deletion of Cdc42 inhibited chondrocyte terminal differentiation.

### 2.4. Effect of Cdc42 deficiency on autopod skeleton

To analyze the phenotype of the autopods in detail, skeleton preparations of fore- and hindlimbs obtained at E14.5, E15.5, E16.5, E18.5, and P0 were stained with Alcian blue and Alizarin red. Ectopic cartilages were found between the 2nd and 3rd digits in $Cdc42^{fl/fl}$; $Prx1$-$Cre$ forelimbs at E14.5 (red arrow in Fig. 4A), whereas no ectopic cartilages were found in the hindlimbs at the same stage (Fig. 4F). At E15.5, E16.5, E18.5 and P0, the autopods showed thick cartilages and abnormal joints, while ectopic cartilages between the
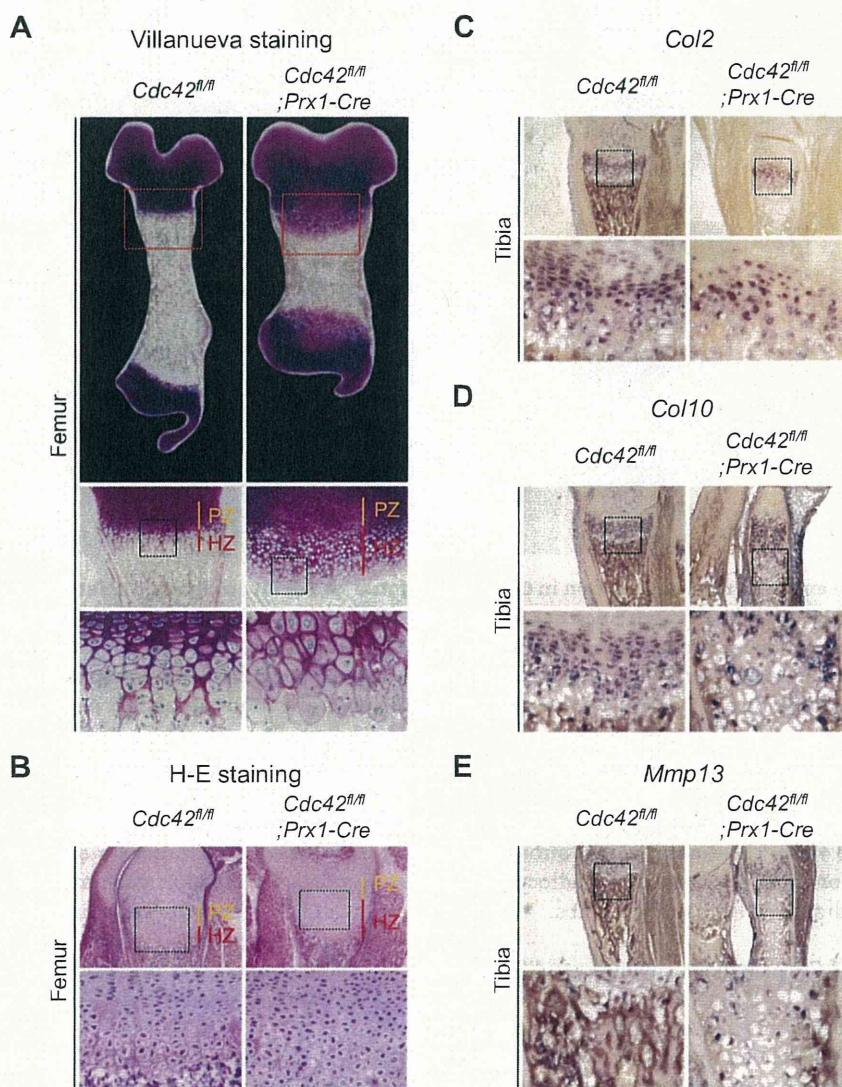


Fig. 3 – Histological analyses of growth plate defects in Cdc42 conditional knockout mice. (A) Villanueva stained sections of femur obtained at P0. Long bones of $Cdc42^{fl/fl}$; $Prx1$-$Cre$ mice were shorter and thicker than those of $Cdc42^{fl/fl}$ mice. PZ, proliferating zone; HZ, hypertrophic zone. (B) Hematoxylin- and Eosin-stained sections of femur obtained at P0. Severe defects were found in growth plate cartilage of $Cdc42^{fl/fl}$; $Prx1$-$Cre$ mice, which was characterized by loss of columnar organization in proliferating chondrocytes and massive accumulation of hypertrophic chondrocytes. PZ, proliferating zone; HZ, hypertrophic zone. (C–E) In situ hybridization analyses for the indicated genes were performed using tibiae obtained at E18.5. Reduced expressions of Col10 (D) and Mmp13 (E) were apparent in $Cdc42^{fl/fl}$; $Prx1$-$Cre$ mice. Boxed areas are enlarged in the lower panels (A–E).
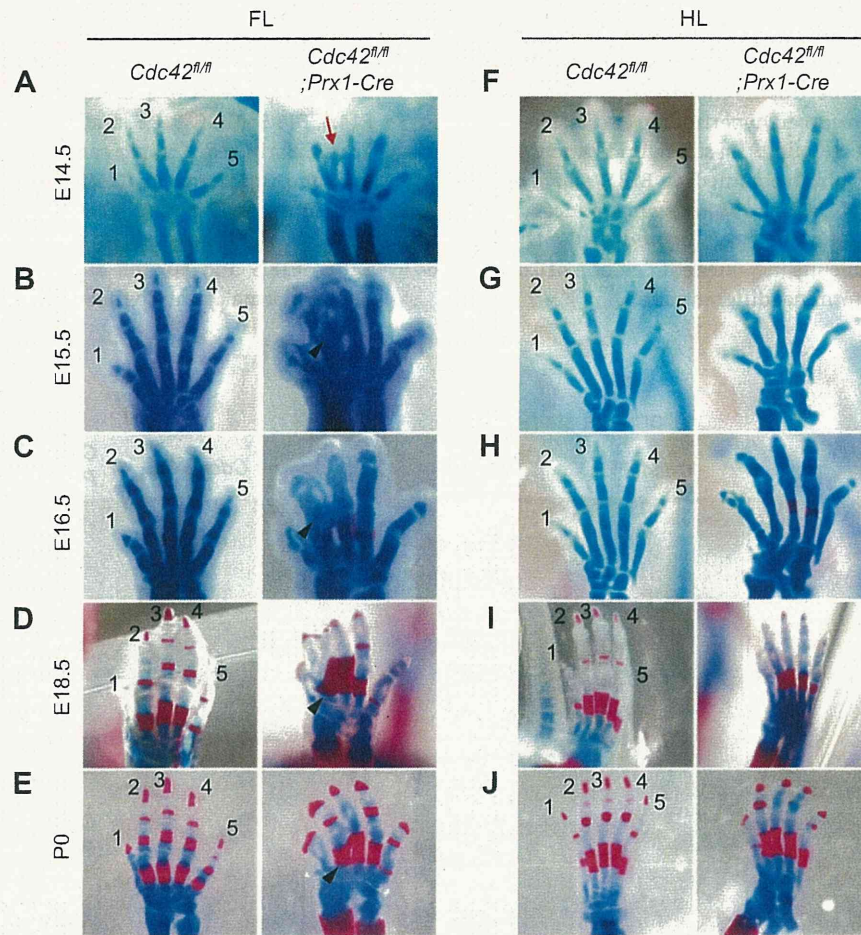
**Fig. 4 – Analysis of endochondral ossification in *Cdc42* conditional knockout autopods. Skeleton preparations of fore- (FL) (A–E) and hindlimbs (HL) (F–J) obtained from mice at E14.5 (A and F), E15.5 (B and G), E16.5 (C and H), E18.5 (D and I), and P0 (E and J) were made. Analyses of those preparations revealed ectopic cartilage between the 2nd and 3rd digits in *Cdc42^{fl/fl}*; *Prx1-Cre* mice (red arrow in A). After E15.5, *Cdc42^{fl/fl}*; *Prx1-Cre* FL showed an abnormal calcification pattern and fusion of the 2nd and 3rd metacarpals (black arrowheads in B–E). On the other hand, fusion of the metacarpals did not appear in *Cdc42^{fl/fl}*; *Prx1-Cre* HL (F–J).**

2nd and 3rd metacarpals were seen only in forelimbs (black arrowheads in Fig. 4B–E). These observations strongly suggest an essential role for *Cdc42* in control of chondrocyte function during endochondral bone formation in limbs.

### 2.5. Deletion of Cdc42 inhibits chondrocyte differentiation

We employed *in vitro* micromass culture assays to further define the underlying chondrogenic defect identified in our *in vivo* analysis. For these experiments, cells were harvested from fore- and hindlimbs at E12.5, and maintained in culture for 7 days. Micromass cultures derived from *Cdc42^{fl/fl}*; *Prx1-Cre* limbs lacked the Alcian blue staining profile (Fig. 5A). We next examined the effect of Cdc42 deficiency on organization of the actin cytoskeleton, as control of actin remodeling is one of the best characterized roles of Rho GTPases and actin dynamics seem to control chondrocyte differentiation (Woods et al., 2007a). Formation of stress fibers was lost in *Cdc42^{fl/fl}*; *Prx1-Cre* (red arrows in Fig. 5B). Quantitative real-time PCR

analyses revealed that deletion of Cdc42 decreased expressions of the chondrocyte differentiation marker genes *Col2* and *Aggrecan*, while proliferation rate between *Cdc42^{fl/fl}* and *Cdc42^{fl/fl}*; *Prx1-Cre* mice derived micromass cultured cells are not different (Fig. 5C and D). These results suggest that changes in actin organization are connected to altered differentiation of chondrocytes.

### 2.6. Reduced interdigital programmed cell death in Cdc42 conditional mutant limbs

We observed that *Cdc42^{fl/fl}*; *Prx1-Cre* mice had webbed limbs (Fig. 2He, Ie, and g), and fusion of the 2nd and 3rd metacarpals, while that of the 3rd and 4th metacarpals was not seen (Fig. 4B–E). Thus, it is possible that the webbed limb condition was caused by not only ectopic cartilage formation and fusion of metacarpals, but also an absence of ID-PCD. In wild-type mice, PCD occurs between E12.5 and E13.5, and eliminates cells in the interdigital region, with only a residual
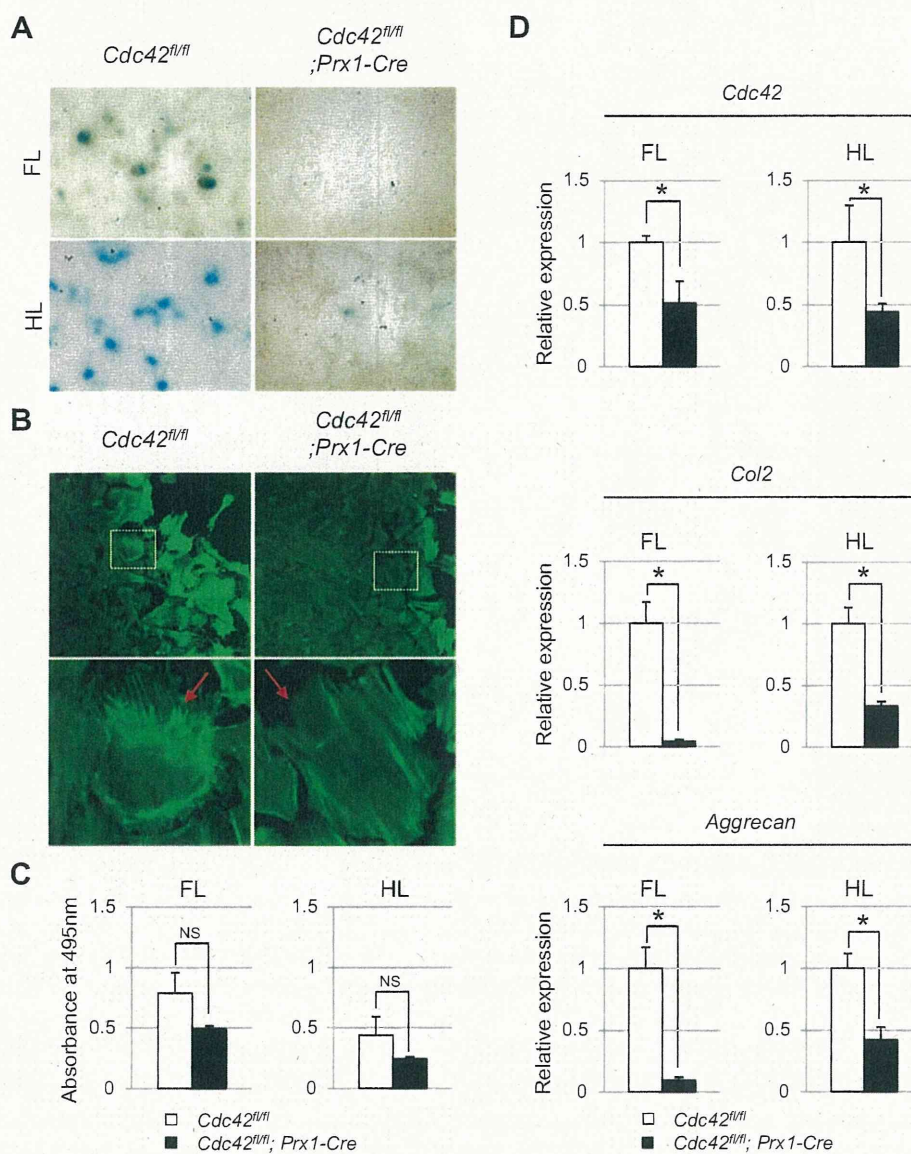
Fig. 5 – Micromass cultures of chondrocyte differentiation and organization of actin cytoskeleton in *Cdc42* conditional knockout mice. (A) Forelimb (FL) and hindlimb (HL) mesenchyme from E12.5 embryos were placed in micromass culture for 7 days, after which time the cells were stained with Alcian blue. (B) Micromass cultures of E12.5 embryos were cultured for 7 days and stained with the anti-Actin antibody. Boxed areas are enlarged and shown in lower panels. A decreased number of stress fibers was seen in cultured cells from *Cdc42*$^{fl/fl}$; *Prx1-Cre* mice as compared with those from *Cdc42*$^{fl/fl}$ mice (red arrows). (C) Cell proliferation in micromass cultures was assessed using an MTT method. Absorbance of MTT-formazan formed in *Cdc42*$^{fl/fl}$ (white column) and *Cdc42*$^{fl/fl}$; *Prx1-Cre* (black column) derived micromass cultured cells. (D) Expression levels of *Cdc42*, *Col2*, and *Aggrecan* were determined using real-time PCR. Amplification signals from target genes were normalized against that from *18S*. Results in (C) and (D) are shown as the mean ± SD (error bars) of 4 independent experiments $^{*}p < 0.05$; NS, not significant.

interdigital space remaining at the most proximal level by E14.5, leading to separation of individual digits (Fernandez-Teran et al., 2006).

To determine whether the webbing in *Cdc42*$^{fl/fl}$; *Prx1-Cre* mice was due to not only ectopic cartilage formation and fusion of metacarpals, but also an absence of ID-PCD, TUNEL assays were performed using limb buds obtained at E12.5–E14.5, which demonstrated a significant reduction in ID-PCD

in the limb buds (Fig. 6A; compare f with i, and l with o). When we counted TUNEL-stained cells in the interdigital regions of the 1st to 2nd, 2nd to 3rd, and 3rd to 4th digits obtained at E13.5 and E14.5, the number of apoptotic cells in *Cdc42*$^{fl/fl}$; *Prx1-Cre* embryos was significantly reduced ($p < 0.01$) as compared to *Cdc42*$^{fl/fl}$ embryos (Fig. 6B). The characteristic *Cdc42*$^{fl/fl}$; *Prx1-Cre* webbing was observed between the 1st and 2nd, 2nd and 3rd, and 3rd and 4th digits, while it was not observed
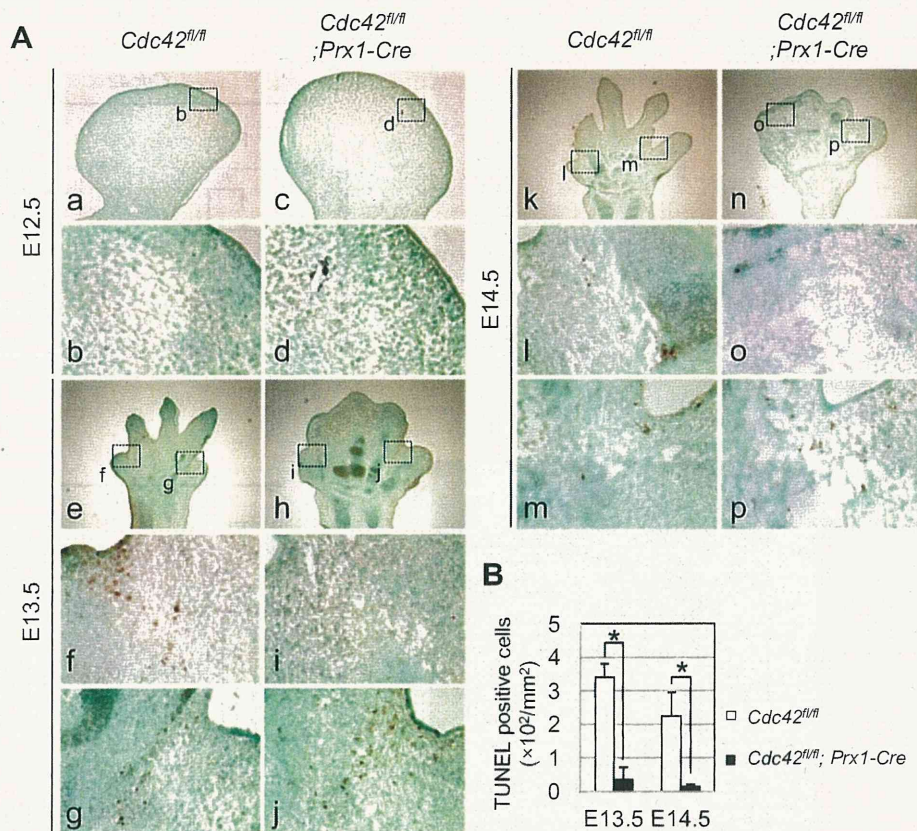
**Fig. 6 – Reduced programmed cell death in interdigital regions of Cdc42 conditional knockout mice. (A) TUNEL assays were performed using forelimbs obtained at E12.5 (a–d), E13.5 (e–j), and E14.5 (k–p). Boxed areas are enlarged and shown in lower panels. There was a significant reduction of interdigital programmed cell death in $Cdc42^{fl/fl}$; Prx1-Cre limbs at E13.5 and E14.5 as compared to $Cdc42^{fl/fl}$ limbs. (B) Numbers of TUNEL-stained cells in interdigital regions between 1st and 2nd, 2nd and 3rd, and 3rd and 4th digits in $Cdc42^{fl/fl}$ and $Cdc42^{fl/fl}$; Prx1-Cre mice at E13.5 and E14.5. Average and standard deviation values for those 3 regions in 3 slides (total 9 regions) are shown for each data point ($^*p < 0.01$).**

between the 4th and 5th digits (Fig. 2H and I). This phenotype was consistent with the results of our TUNEL assays, which demonstrated no significant reduction of ID-PCD between the 4th and 5th digits in those limbs (Fig. 6A; compare g with j, and m with p). These findings suggest that ID-PCD in $Cdc42^{fl/fl}$; Prx1-Cre limb buds is incomplete as compared to $Cdc42^{fl/fl}$ mice, while the Cdc42 phenotype may be associated with ID-PCD in the limbs.

### 2.7. Expressions of limb-patterning genes in Cdc42 conditional knockout limb buds

We performed a comprehensive analysis of the candidate gene set by comparing expression patterns in the limb buds of $Cdc42^{fl/fl}$ and $Cdc42^{fl/fl}$; Prx1-Cre mice using whole-mount in situ hybridization analyses. Expressions of Fgf8, an AER marker, and Sonic hedgehog (Shh), a zone of polarizing activity (ZPA) marker, were clearly present and appeared to be correctly positioned in the $Cdc42^{fl/fl}$; Prx1-Cre limb buds at E11.5 (Fig. 7A and B). These results indicate that loss of Cdc42 in the limb bud mesoderm does not affect the formation of AER and ZPA. Furthermore, we analyzed the expression of Sox9, a master transcription factor during condensation

of the skeletal anlagen. Sox9 was ectopically expressed between the 2nd and 3rd digits of the $Cdc42^{fl/fl}$; Prx1-Cre limbs at E12.5 (yellow arrowhead in Fig. 7C). These results indicate that ectopic Sox9 expression is associated with deformity of the limbs in $Cdc42^{fl/fl}$; Prx1-Cre mice.

### 2.8. Expressions of Bmps and Msxs in Cdc42 conditional knockout limb buds

It has been reported that several BMP family members have multiple roles in limb development, including AER maintenance, skeletal formation, and apoptosis in the interdigital regions (Bandyopadhyay et al., 2006; Robert, 2007). Therefore, we analyzed the expressions of genes related to mesenchymal BMP signaling to determine whether the webbed limbs of $Cdc42^{fl/fl}$; Prx1-Cre mice might be explained by interdigital BMP signaling. Whole-mount in situ hybridization analyses revealed reduced interdigital and peri-digital expressions of Bmp2 at E12.5 and E13.5 in $Cdc42^{fl/fl}$; Prx1-Cre limbs (red arrowheads in Fig. 8A). Ectopic expression of Bmp7 also appeared in the limb buds of $Cdc42^{fl/fl}$; Prx1-Cre mice as compared to those of $Cdc42^{fl/fl}$ mice (yellow arrowheads in Fig. 8B). The closely related homeobox genes Msx1 and Msx2
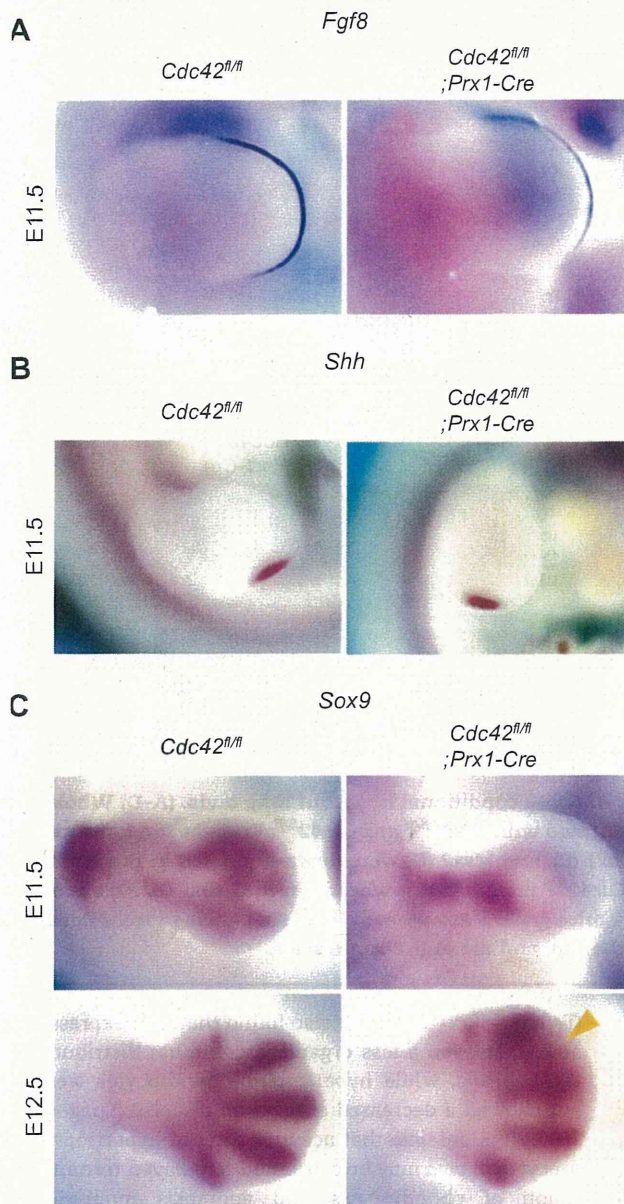
**A**

*Fgf8*



**B**

*Shh*



**C**

*Sox9*



Fig. 7 – Expressions of limb-patterning genes in *Cdc42* conditional knockout limb buds. (A–C) Whole-mount *in situ* hybridization analyses of the indicated genes were performed using $Cdc42^{fl/fl}$ and $Cdc42^{fl/fl}$; *Prx1-Cre* forelimb buds at the indicated embryonic stages. The results showed no significant differences for the expressions of *Fgf8* (A) and *Shh* (B). An abnormal expression pattern of *Sox9* was apparent in $Cdc42^{fl/fl}$; *Prx1-Cre* mice (yellow arrowhead in C). All panels present dorsal views of $Cdc42^{fl/fl}$ and $Cdc42^{fl/fl}$; *Prx1-Cre* forelimb buds, anterior to the top, and are at the same scale.

are key downstream targets of BMP signaling, and expressed in the PCD zones of developing limbs, including the interdigital regions (Houzelstein et al., 1997). Expressions of *Msx1* and *Msx2* were reduced in the $Cdc42^{fl/fl}$; *Prx1-Cre* limbs at E12.5 and E13.5 as compared to $Cdc42^{fl/fl}$ mice (red arrowheads in Fig. 8C

and D). Our results indicate that abnormal or insufficient expressions of *Bmp2*, *Bmp7*, *Msx1*, and *Msx2* may cause a lack of ID-PCD, which is associated with syndactyly in $Cdc42^{fl/fl}$; *Prx1-Cre* mice.

## 3.     Discussion

Recent studies that utilized tissue- and cell-type specific gene targeting of *Cdc42* in mice have revealed definitive information regarding the physiological functions of various tissues (Melendez et al., 2011). However, the roles of Cdc42 in skeletogenesis, especially during limb development, are not fully understood. These are the first results to demonstrate that Cdc42 plays a critical role in early chondrogenesis, including mesenchymal condensation, followed by differentiation of cells into chondrocytes and ID-PCD during limb development.

It is intriguing that the abnormalities of ID-PCD followed by soft tissue syndactyly appear in both $Cdc42^{fl/fl}$; *Prx1-Cre* and $Rac1^{fl/fl}$; *Prx1-Cre* mice (Suzuki et al., 2009). A hierarchical relationship has been proposed, in which Cdc42 is a proximal mediator that signals to Rac1 (Hall, 1998). Cdc42 and Rac1 share some effectors, including p21 activated kinases (Paks), and participate together in regulation of important cellular functions (Bishop and Hall, 2000; Etienne-Manneville and Hall, 2002). In the present as well as previous studies, downregulation of Msx1 and Msx2 was shown to be correlated with a decrease in apoptosis in the interdigital regions of both $Cdc42^{fl/fl}$; *Prx1-Cre* and $Rac1^{fl/fl}$; *Prx1-Cre* limb buds (Suzuki et al., 2009). Msx1 and Msx2 are considered to be downstream target genes of BMP signaling, and these results suggest that Cdc42 and Rac1 might share functions of limb bud ID-PCD via BMP signaling.

On the other hand, comparison of the phenotypes observed in $Cdc42^{fl/fl}$; *Prx1-Cre* and $Rac1^{fl/fl}$; *Prx1-Cre* mice indicate that the functions of Cdc42 and Rac1 do not completely overlap during palate (Fig. 2D and E) and forelimb (Fig. 4A–E) development (Suzuki et al., 2009). Most of the $Cdc42^{fl/fl}$; *Prx1-Cre* mice exhibited a cleft palate, whereas $Rac1^{fl/fl}$; *Prx1-Cre* mice did not. Furthermore, all of the $Cdc42^{fl/fl}$; *Prx1-Cre* mice exhibited fusion of the metacarpals, whereas the $Rac1^{fl/fl}$; *Prx1-Cre* mice exhibited no fusion between bones of adjacent digits. Cdc42 regulates chondrogenesis at stages later than condensations in ATDC5 cells, while Rac1 signaling regulates chondrogenesis by exerting its effects at the stage of cellular condensation formation (Woods et al., 2007b). However, our results suggest that Cdc42, but not Rac1, regulates chondrogenesis during mesenchymal condensation. In many cases, results with knockout mice correlate with those observed *in vitro*, but, analysis of knockout mice sometimes gives opposite effects to what has been predicted from *in vitro* study. Additional studies are needed to identify signaling molecules regulated by Cdc42 and Rac1 in limb bud mesenchyme.

Chondrocyte differentiation is characterized by drastic changes in cell shape and size, thus organization of the actin cytoskeleton plays an important role in this process. Wang et al. demonstrated that over-expression of Cdc42 in the chondrocyte cell line ATDC5 resulted in filopodia formation, followed by earlier induction of hypertrophic markers, such
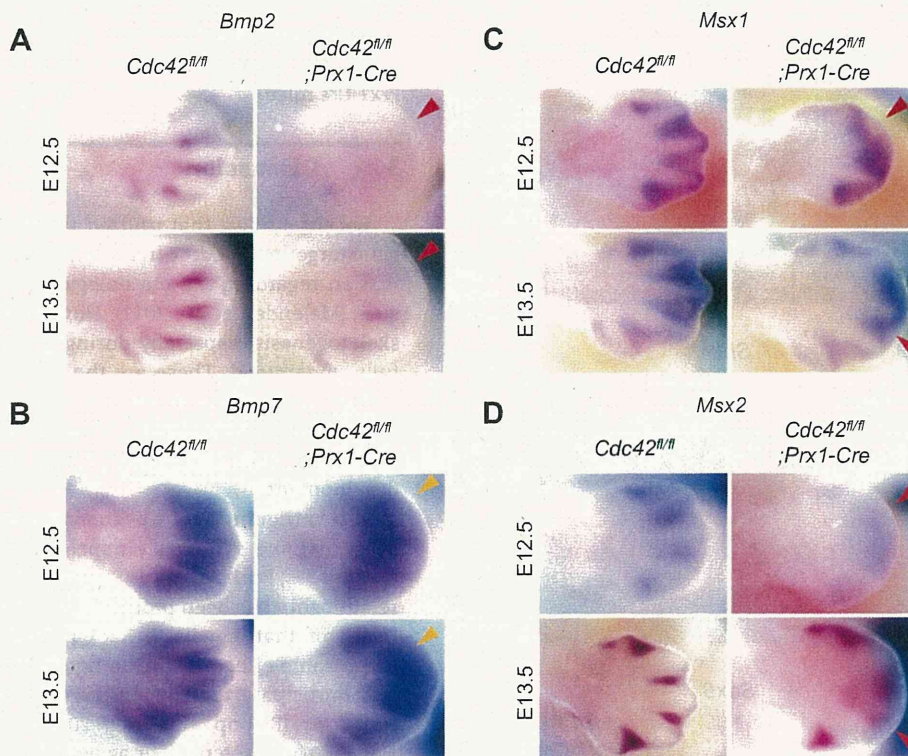
Fig. 8 – Expressions of *Bmps* and BMP signaling target genes in *Cdc42* conditional knockout limb buds. (A–D) Whole-mount *in situ* hybridization analyses of the indicated genes were performed with *Cdc42$^{fl/fl}$* and *Cdc42$^{fl/fl}$*; *Prx1-Cre* forelimb buds at the indicated embryonic stages. The expressions of *Bmp2* (A), *Msx1* (C), and *Msx2* (D) were down-regulated in the interdigital regions of *Cdc42$^{fl/fl}$*; *Prx1-Cre* limbs as compared to those of *Cdc42$^{fl/fl}$* mice (red arrowheads in A, C, and D). An abnormal expression pattern of *Bmp7* was apparent in *Cdc42$^{fl/fl}$*; *Prx1-Cre* mice (yellow arrowheads in B). All panels present dorsal views of *Cdc42$^{fl/fl}$* and *Cdc42$^{fl/fl}$*; *Prx1-Cre* forelimb buds, anterior to the top, and are at the same scale.

as Col10 expression and matrix mineralization. These results suggest that Cdc42 signaling is required for normal hypertrophic differentiation of chondrocytes accompanied by changes in actin organization and cell morphology (Wang and Beier, 2005). In our experiments, micromass cultures derived from *Cdc42$^{fl/fl}$*; *Prx1-Cre* limb buds developed less cortical actin organization. Zanetti et al. suggested that disrupted actin formation using the actin binding drug cytochalasin D induced immediate cell rounding and subsequent accelerated terminal differentiation of chondrocytes (Zanetti and Solursh, 1984). Analyses of micromass cultures partially supported our *in vivo* data, suggesting that deletion of Cdc42 within embryonic limb mesenchyme of *Cdc42$^{fl/fl}$*; *Prx1-Cre* embryos leads to defects in cartilage condensation and formation of mature cartilage elements.

*Cdc42$^{fl/fl}$*; *Prx1-Cre* mice displayed an expansion of hypertrophic cartilage in growth plates (Fig. 3A and B), while expressions of Col10 and Mmp13 were clearly decreased (Fig. 3D and E), indicating functional derangement. Transgenic mice mis-expressing Sox9 in hypertrophic chondrocytes showed features in growth plates that were similar to those of *Cdc42$^{fl/fl}$*; *Prx1-Cre* mice, including delayed endochondral bone formation associated with reduced bone growth due to deficiencies of vascular invasion into hypertrophic cartilage and cartilage resorption (Hattori et al., 2010). A study of TGF-β type II receptor (Tgfbr2) conditional knockout mice

(*Tgfbr2$^{fl/fl}$*; *Prx1-Cre* mice) also found that Col2 expressing cells at P0 displayed a less organized columnar distribution than the controls, while hypertrophic chondrocytes were larger but showed a decreased expression of Col10 (Spagnoli et al., 2007). It is possible that accumulation of hypertrophic chondrocytes *in vivo* may be attributed to delayed terminal maturation of chondrocytes and apoptosis induced in the chondro-osseous junction in *Cdc42$^{fl/fl}$*; *Prx1-Cre* mice (Shapiro et al., 2005; Zhang et al., 2011).

Recently, the significance of CDC42 during development has been shown in several human diseases and syndromes. Interestingly, ARHGAP31, a candidate gene for Adams–Oliver syndrome (AOS), characterized by a combination of aplasia cutis congenital (ACC) and terminal transverse limb defects (TTLD), was shown to be a CDC42 GTPase regulator, which plays a key role in controlling temporal and spatial cytoskeletal remodeling necessary for precise control of cell morphology and migration (LaLonde et al., 2006). Gain-of-function mutations of ARHGAP31 in humans who possess phenotypes of limb abnormalities typically have effects on the distal phalanges or entire digits, or rarely, more proximal limb structures (Southgate et al., 2011). In addition, recessive mutations in DOCK6, which encodes an atypical guanidine exchange factor (GEF) known to activate CDC42, lead to AOS (Shaheen et al., 2011). Phenotypes of this syndrome are identical to those of *Cdc42$^{fl/fl}$*; *Prx1-Cre* mice.

In conclusion, our results demonstrated that Cdc42 is required for chondrogenesis and interdigital programmed cell death during limb development.

## 4. Experimental procedures

### 4.1. Generation of mice

The animal experiments were conducted in accordance with the guidelines of Showa University and University of Tokyo. The targeting vector consisted of loxP-flanked exon 2 (first coding exon) of the Cdc42 gene and FRT-flanked neo gene, both of which were linked between the 5'- and 3'-homologous sequences of the Cdc42 locus. The targeting vector was transfected into embryonic stem cells and homologous recombinants were identified by Southern blot analysis. Chimeric mice were generated by injecting targeted ES cell clones into blastocysts, then crossed with Actin-Flp transgenic mice (Rodriguez et al., 2000) for excision of the neo gene via Flp-FRT recombination. Cdc42 was knocked out via Cre-loxP recombination by crossing Cdc42 flox with Prx1-Cre transgenic (Prx1-Cre) mice (Logan et al., 2002). Offspring were genotyped by PCR analysis using the following primer pairs: for Prx1-Cre, 5'-GACGATGCAACGAGTGATGA-3' and 5'-AGCAT TGCTGTCACTTGGTC-3'; for Cdc42, F1 5'-ATCGGTCACTGTTC-TACTTTG-3' and R1 5'-TACTGCTATGACTGAAAACCTC-3'. Both conditional and Δexon2 alleles were identified using the following primers, F1, R1, and R2 5'-GTTTT GCCTGCATG-TATGTCTG-3' (Fig. 1A). The genetic background of the mice used in this study is a hybrid of C57BL/6, 129Ola, and ICR. In an analysis of the expression pattern of Prx1-mediated Cre recombination, both Prx1-Cre transgenic line and R26R conditional reporter allele were previously described (Soriano, 1999). Mating Prx1-Cre and R26R mice generated transgenic mice (R26R; Prx1-Cre mice). Detection of β-galactosidase (lacZ) activity in both whole embryos and tissue sections was performed as previously described (Chai et al., 2000).

### 4.2. Western blot analysis

Western blot analysis was performed as previously described (Yamada et al., 2005). Briefly, sample lysates were subjected to 15% SDS–PAGE and transferred to Immobilon-P membranes (Millipore). The membranes were then incubated with antibodies against mouse Cdc42 (Active Cdc42 Pull-Down and Detection Kit, Thermo Scientific), following incubation with a horseradish peroxidase-conjugated secondary antibody (GE Healthcare UK Ltd.). Protein bands were detected using an ECL plus Western blot detection system (GE Healthcare UK Ltd.) and exposed to medical X-ray film (FUJIFILM).

### 4.3. Whole-mount in situ hybridization

Whole-mount in situ hybridization was performed using embryos according to a method previously reported (Sagai et al., 2005). Briefly, digoxigenin-labeled riboprobes were transcribed in vitro according to the manufacturer's protocol (Roche Diagnostics Co.). For the Cdc42 probe, 1724-bp mouse Cdc42 cDNA containing the whole coding sequence was generated by RT-PCR using oligonucleotides, 5'-GGCGGAGAAGCT-

GAGGACAA-3' and 5'-CACCCCATGCTCATAGCTTC-3', then cloned into pCRII-TOPO (Invitrogen) and linearized with Xho I to synthesize the antisense probe. With this probe, we were able to detect Cdc42 mRNA transcribed from not only exon2 (region deleted by Prx1-Cre), but also other exons containing a whole coding sequence. In addition, the following probes were used: Sox9 (Suzuki et al., 2009), Bmp2 (gifted from Dr. Y. Takahashi), Bmp7 (gifted from Dr. P.J. Hurlin), Msx1 and Msx2 (gifted from Dr. R.E. Hill), Fgf8 (gifted from Dr. G.R. Martin), and Shh (gifted from Dr. A.P. McMahon). The numbers of embryos used for measurements were as follow (values for $Cdc42^{fl/fl}$ and $Cdc42^{fl/fl}$; Prx1-Cre, respectively, shown in parentheses): Cdc42 (4 and 4), Sox9 (7 and 7), Bmp2 (4 and 4), Bmp7 (4 and 4), Msx1 (6 and 6), Msx2 (4 and 4), Fgf8 (3 and 3), and Shh (3 and 3). All results of analyses of the indicated genes were nearly uniform.

### 4.4. Anatomical and histological analyses

For skeletal staining, mice were skinned, eviscerated, and dehydrated in 95% ethanol overnight. The skeletons were then stained overnight with 0.015% Alcian blue and 10% acetic acid in 75% ethanol, and soft tissues were dissolved overnight in 2% KOH, while the skeletons were additionally stained overnight with 0.0075% Alizarin red in 1% KOH. Finally, the skeletons were cleared in 0.5% KOH and 20% glycerol for several days, and stored in glycerol/ethanol (1:1). For general morphological examinations, all samples were fixed in 4% paraformaldehyde and processed into serial paraffin sections using routine procedures. Deparaffinized sections were stained with Hematoxylin and Eosin or Villanueva. In situ hybridization of paraffin sections processed from mice tibiae for Col2, Col10, and Mmp13 was performed using DIG-labeled RNA proves, The following probes were used: Col2 and Col10 (gifted from Dr. S. Takeda), and Mmp13 (gifted from Dr. T. Hattori). The numbers of embryos used for measurements were as follow (values for $Cdc42^{fl/fl}$ and $Cdc42^{fl/fl}$; Prx1-Cre, respectively, shown in parentheses): Col2 (7 and 7), Col10 (7 and 5) and Mmp13 (7 and 7). All results of analyses of the indicated genes were nearly uniform.

### 4.5. Micro-CT scanning

Scanning was performed using a microfocus X-ray computed tomography system, according to the manufacturer's protocol (inspeXio SMX-90CT, Shimadzu, Japan), with a tube voltage of 90 kV and tube current of 110–90 μA.

### 4.6. Micromass culture

E12.5 limb buds were collected in Dulbecco's modified PBS at 4 °C. Mesenchymal cells were dissociated in Dulbecco's modified PBS containing 0.1% trypsin, 0.4 mM EDTA, and 0.1% collagenase at 37 °C for 10 min, then resuspended in D-MEM/Ham's F-12 (Wako) with 10% fetal bovine serum, 1 mM β-Glycerophosphate, 50 μg/ml L-ascorbic acid, 50 U/ml penicillin, and 50 mg/ml streptomycin at $2 \times 10^7$ cells/ml. Next 10-μl drop of the cell suspension were placed in the center of wells in a standard 48-well polystyrene tissue culture dish. Cells were allowed to adhere for 2 h at 37 °C and 5% $CO_2$, and

1 ml of medium was added to the culture. Alcian blue staining and immunocytochemistry using the antibody against actin (Molecular Probes) were performed as previously described (Furusawa et al., 2006).

### 4.7. MTT assay

An MTT assay was performed using a CellTiter 96 Aqueous One Solution cell proliferation assay, according to the manufacturer's protocol (Promega).

### 4.8. Quantitative real-time PCR

Total RNA samples were extracted and reverse-transcribed using a Fast SYBR Green Cells-to-Ct Kit (Invitrogen). Quantitative real-time PCR was performed using a SYBR green Fast PCR system (GE Healthcare UK Ltd.), with the following primer sequences:

Cdc42, 5'-GAAACTTGCCAAGAACAAACAGAA-3' and 5'-CCG CGCCAGCTTTTCA-3'
Col2, 5'-GCTCCCAGAACATCACCTACCA-3' and 5'-TACATT GGAGCCCTGGATGAG-3'
Aggrecan, 5'-CAGCTGCCCTTCACATGTAAA-3' and 5'-TGG ACAAAGCCCTCAGTACACT-3'
18S, 5'-AACTTTCGATGGTAGTCGCCG-3' and 5'-CCTTGGAT GTGGTAGCCGTTT-3'.

### 4.9. Cell death analysis

Embryos were rinsed with PBS, placed in sterile molds, and embedded in the frozen tissue embedding medium OCT compound (Tissue-Tek OCT compound, Sakura Finetechnical Co., Ltd.). Frozen sections were cut on a cryostat at 8 μm and mounted on pre-cleaned microscope glass slides (StarFrost, Muto Pure Chemicals Co., Ltd.). Assays of cell death were performed using TdT-mediated dUTP nick-end-labeling (TUNEL) analysis of frozen sections, according to the manufacturer's protocol (Wako Pure Chemical Industries, Ltd.). Three sections were selected from each slide (3 slides; total 9 sections). For statistical analysis, the 2-tailed Student's t test was used. $p$ Values less than 0.05 were considered significance.

## Appendix A. Supplementary data

Supplementary data associated with this article can be found, in the online version, at doi:10.1016/j.mod.2012.02.002.

REFERENCES

Bandyopadhyay, A., Tsuji, K., Cox, K., Harfe, B.D., Rosen, V., Tabin, C.J., 2006. Genetic analysis of the roles of BMP2, BMP4, and BMP7 in limb patterning and skeletogenesis. PLoS Genet. 2, e216.

Bastida, M.F., Sheth, R., Ros, M.A., 2009. A BMP-Shh negative-feedback loop restricts Shh expression during limb development. Development 136, 3779–3789.

Bishop, A.L., Hall, A., 2000. Rho GTPases and their effector proteins. Biochem. J. 348 (Pt 2), 241–255.

Burridge, K., Wennerberg, K., 2004. Rho and Rac take center stage. Cell 116, 167–179.

Capdevila, J., Izpisua Belmonte, J.C., 2001. Patterning mechanisms controlling vertebrate limb development. Annu. Rev. Cell Dev. Biol. 17, 87–132.

Chai, Y., Jiang, X., Ito, Y., Bringas Jr., P., Han, J., Rowitch, D.H., Soriano, P., McMahon, A.P., Sucov, H.M., 2000. Fate of the mammalian cranial neural crest during tooth and mandibular morphogenesis. Development 127, 1671–1679.

Chen, F., Ma, L., Parrini, M.C., Mao, X., Lopez, M., Wu, C., Marks, P.W., Davidson, L., Kwiatkowski, D.J., Kirchhausen, T., Orkin, S.H., Rosen, F.S., Mayer, B.J., Kirschner, M.W., Alt, F.W., 2000. Cdc42 is required for PIP(2)-induced actin polymerization and early development but not for cell viability. Curr. Biol. 10, 758–765.

Chen, Y., Zhao, X., 1998. Shaping limbs by apoptosis. J. Exp. Zool. 282, 691–702.

DeLise, A.M., Fischer, L., Tuan, R.S., 2000. Cellular interactions and signaling in cartilage development. Osteoarthritis Cartilage 8, 309–334.

Erlebacher, A., Filvaroff, E.H., Gitelman, S.E., Derynck, R., 1995. Toward a molecular understanding of skeletal development. Cell 80, 371–378.

Etienne-Manneville, S., Hall, A., 2002. Rho GTPases in cell biology. Nature 420, 629–635.

Fernandez-Teran, M.A., Hinchliffe, J.R., Ros, M.A., 2006. Birth and death of cells in limb development: a mapping study. Dev. Dyn. 235, 2521–2537.

Francis-West, P.H., Antoni, L., Anakwe, K., 2003. Regulation of myogenic differentiation in the developing limb bud. J. Anat. 202, 69–81.

Furusawa, T., Lim, J.H., Catez, F., Birger, Y., Mackem, S., Bustin, M., 2006. Down-regulation of nucleosomal binding protein HMGN1 expression during embryogenesis modulates Sox9 expression in chondrocytes. Mol. Cell. Biol. 26, 592–604.

Hall, A., 1998. Rho GTPases and the actin cytoskeleton. Science 279, 509–514.

Hall, B.K., Miyake, T., 2000. All for one and one for all: condensations and the initiation of skeletal development. BioEssays 22, 138–147.

Hattori, T., Muller, C., Gebhard, S., Bauer, E., Pausch, F., Schlund, B., Bosl, M.R., Hess, A., Surmann-Schmitt, C., von der Mark, H., de Crombrugghe, B., von der Mark, K., 2010. SOX9 is a major negative regulator of cartilage vascularization, bone marrow